Semimetallic Transport in Nanocomposites Derived from Grafting of Linear and Hyperbranched Poly(phenylene sulfide)s onto the Surface of Functionalized Multi-Walled Carbon Nanotubes

In-Yup Jeon,[†] Hwa-Jeong Lee,[†] Yeong Suk Choi,[‡] Loon-Seng Tan,[§] and Jong-Beom Baek*,[†,||]

School of Chemical Engineering, Chungbuk National University, Cheongju, Chungbuk, 361-763 South Korea, Energy and Environment Laboratory, Samsung Advanced Institute of Technology, Suwon, 449-600 South Korea, Nanostructured & Biological Materials Branch, Materials & Manufacturing Directorate, AFRL/RXBN, Air Force Research Laboratory, Wright-Patterson Air Force Base, Dayton, Ohio 45433-7750, and Ulsan National Institute of Science & Technology (UNIST), Ulsan, 689-805 South Korea

Received June 5, 2008; Revised Manuscript Received August 27, 2008

ABSTRACT: The semimetallic conductive nanocomposites, linear or hyperbranched poly(phenylene sulfide) (PPS) grafted multiwalled carbon nanotubes (MWNT), were successfully prepared by two-step reaction sequences. MWNT were first functionalized with 4-chlorobenzoic acid in poly(phosphoric acid) (PPA)/phosphorus phentoxide (P_2O_5) medium in a "direct" Friedel−Crafts acylation reaction to afford 4-chlorobenzoyl-functionalized MWNT (CB-MWNT). A subsequent nucleophilic substitution reaction between CB-MWNT and 4-chlorobenzenethiol as an AB monomer or 3,5-dichlorobenzenethiol as an AB_2 monomer was conducted to graft the linear PPS (LPPS) or hyperbranched PPS (HPPS) in NMP/toluene in the presence of sodium carbonate to afford LPPS grafted MWNT (LPPS-*g*-MWNT) or HPPS grafted MWNT (HPPS-*g*-MWNT), respectively. The covalent attachment of corresponding polymers onto the surface of MWNT was indirectly confirmed by a model study. The structures of polymer-grafted nanocomposites were clearly discernible from those of the samples prepared by solution-blending of LPPS and CB-MWNT. The dispersability and melt-processability of nanocomposites were enhanced by the grafting of PPS polymers. Thus, the nanocomposite specimens could be easily compression molded. Without chemical doping, the measured surface conductivities of as-prepared LPPS-*g*-MWNT and HPPS-*g*-MWNT molded samples were in the semimetallic transport region at 11.76 and 3.56 S/cm, respectively.

Introduction

Carbon nanotubes (CNTs) continue to attract research and development attention due to their promise of outstanding mechanical, electrical and thermal properties. They can be used as reinforcing additives to various polymer matrices, and the resultant nanocomposites are expected to display enhanced properties.[1] For example, the high aspect ratio of CNTs have resulted in significantly lowering the electrical conductivity percolation threshold (Φ_c) to below 1 vol % in various isotropically blended polymer nanocomposites.[2−7] Therefore, in consideration of CNT-polymer composites for uses as smart structural materials, apart from addressing the issues related to dispersion[8] and interfacial adhesion,[9] it is equally important that the electrical conductivity, which is a key property for application areas, such as self-health monitoring, electro-actuation, etc., be optimized.

In a common practice to improving the dispersion of CNTs in polymer matrices, CNTs are treated in strong, oxidizing acids such as sulfuric acid, nitric acid, or mixture of both acids to generate surface groups such as COOH for subsequent modification.[10] However, it has been shown that if single-walled carbon nanotubes (SWNTs) were not carefully purified first, a majority of COOH functionality created from the treatment of SWNT samples with nitric acid is likely to be on the outer, carbonaceous coats.[11] The sonication treatment, even in neutral water at room temperature, also tends to impart structural damage to CNTs,[12] and dispersing CNTs in slightly acidic conditions with concomitant sonication would accelerate the damage, leading to shortened tubes.[13] Significant damage from these approaches, such as sidewall opening, tube breakage, etc., introduces the defects in CNT that adversely impact the material properties such as electric conductivity, thermal conductivity, and mechanical properties.[14] In this context, less destructive chemical modification of various carbon nanomaterials via electrophilic substitution reaction in a mild poly(phosphoric acid (PPA)/phosphorus pentoxide (P_2O_5) medium has been developed.[15] Although there is little structural damage in the functionalized multiwalled carbon nanotubes (F-MWNT) in such reaction medium, the covalent attachment of organics onto the sidewall of MWNT could disrupt the electronic continuum and reduce their surface electrical and thermal conductivities. Thus, the covalent grafting of a conductive polymer or its precursor onto the surface of F-MWNT could be a viable approach to minimize compromising the electrical conductivity. Our approach involves two-step sequences to generate electrically conductive nanocomposites based on poly(phenylene sulfide), or PPS. PPS is selected as the conductive polymer precursor (conductivity $\sim 10^{-14}$ S/m in undoped state),[16] because it is a well-known engineering thermoplastic resin that displays exceptional mechanical properties, good dimensional stability, good solvent and chemical resistance, and high temperature resistance.[17] Its electrical conductivity could be drastically increased (to $>10^{-3}$ S/cm) upon doping with, for example, AsF_5.[18] The two-step sequences entail the syntheses of a linear PPS (LPPS) from 4-chlorobenzenethiol (AB monomer) and a

* Corresponding author. Telephone: +82-52-708-7034. Fax: + 82-52-708-7010. E-mail: jbbaek@unist.ac.kr.
[†] School of Chemical Engineering, Chungbuk National University.
[‡] Energy and Environment Laboratory, Samsung Advanced Institute of Technology.
[§] Nanostructured & Biological Materials Branch, Materials & Manufacturing Directorate, AFRL/RXBN, Air Force Research Laboratory, Wright-Patterson Air Force Base.
[||] Ulsan National Institute of Science & Technology (UNIST).

10.1021/ma801259b CCC: $40.75
Published on Web 10/04/2008

hyperbranched PPS (HPPS) from 3,5-dichlorobenzenethiol (AB_2 monomer) and under appropriate conditions, they are grafted from the 4-chlorobenzoyl pendants (grafting sites) on MWNT (CB-MWNT), which has been previously generated from the reaction between 4-chlorobenzoic acid and MWNT via an electrophilic substitution reaction in PPA/P_2O_5 medium.[19] The nanocomposites thus obtained display good electrical conductivity because of MWNT while bestowed with good melt-processability due to the presence of PPS.

Experimental Section

Materials. All reagents and solvents were purchased from Aldrich Chemical Inc. or Tokyo Chemical Inc. and used as received, unless otherwise mentioned. *N*-methyl-2-pyrrolidinone (NMP, Fisher Chemical Co.) was distilled from phosphorus pentoxide under reduced pressure. Multiwalled carbon nanotubes (MWNT, CVD MWNT 95 with diameters of 10−20 nm and lengths of 30−50 μm) were obtained from Iljin Nanotech Co., LTD, Seoul, Korea.[20]

Instrumentation. Infrared (IR) spectra were recorded on Jasco FT-IR 480 Plus spectrophotometer. Solid samples were imbedded in KBr disks. Elemental analysis (EA) was performed by system support at Chungbuk National University (CBNU) with a CE Instruments EA1110. Differential scanning calorimetry (DSC) was performed under nitrogen atmosphere with heating and cooling rates of 10 °C/min using a Perkin-Elmer DSC7 equipped with TAC7 controller. The DSC thermograms were obtained on powder samples after they had been heated to 300−350 °C and cooled to 20 °C. Glass transition temperatures (T_g's) were taken as the midpoint of the baseline shift. Thermogravimetric analysis (TGA) was conducted both in air and nitrogen atmospheres with a heating rate of 10 °C/min using a Perkin-Elmer TGA7. The powder patterns of X-ray diffraction (XRD) were recorded with a Scintag DMS 2000 diffractometer using Ni-filtered Cu Kα radiation (40 kV, 100 mA, $\lambda = 0.15418$ nm). The field emission scanning electron microscopy (FE-SEM) used in this work was LEO 1530FE. The field emission transmission electron microscope (FE-TEM) employed in this work was a FEI Tecnai G2 F30 S-Twin. The resistance of samples was measured by four point probe method using Advanced Instrument Technology (AIT) CMT-SR1000N with Jandel Engineering probe at room temperature. The conductivity values were the averages of 10 measurements.

Functionalization of MWNT with 4-Chlorobenzoic Acid. In a resin flask equipped with high torque mechanical stirrer, nitrogen inlet and outlet, 4-chlorobenzoic acid (5.0 g, 31.9 mmol), MWNT (5.0 g), PPA (200.0 g, 83% P_2O_5 assay) and P_2O_5 (50.0 g) were placed. The flask immersed in oil bath and the temperature was raised to 80 °C and stirred at the temperature for 2 h. The reaction mixture was stirred and further heated to 100 °C for 1 h. Then, it was heated to 130 °C for 72 h. At the end of reaction, the dark homogeneous mixture was precipitated in water. The precipitates were collected by suction filtration and Soxhlet extracted with water for three days and with methanol for three days more, and finally freeze-dried for 48 h to afford 5.2 g (55% yield) of dark black powder: Anal. Calcd for $C_{224.26}H_4ClO$ (calculation based on % yield): C, 97.98; H, 0.15. Found: C, 95.47; H, 0.19.

Model Reaction of CB-MWNT with 4-Methylbenzenethiol. In a 100 mL, three-necked, round-bottom flask equipped with a magnetic stirrer, a reflux condenser, a Dean−Stark trap, a nitrogen inlet and outlet, CB-MWNT (0.5 g), 4-methylbenzenethiol (0.5 g, 4.03 mmol), sodium carbonate (0.5 g, 4.72 mmol), toluene (20 mL), and *N*-methyl-2-pyrrolidinone (10 mL) were charged. The mixture was then heated to 160 °C for 2 h. The water generated during the reaction was removed by azeotropic distillation with toluene. The mixture was further heated to 180 °C for 2 h to complete dehydration. The mixture was cooled to 160 °C and stirred at the temperature for additional 6 h. The mixture was poured into 500 mL of distilled water containing 50 mL of conc. hydrochloric acid. The precipitates were washed with water and collected by suction filtration. The resultant solids were transferred to an extraction thimble and Soxhlet-extracted with water for three days and methanol for three more days, and finally freeze-dried for 48 h to give 0.52 g of 4-(4-methylbenzenethio)benzoyl-functionalized MWNT (MB-MWNT) as a black powder.

Representative Polymerization Procedure. In a 100 mL, three-necked, round-bottom flask equipped with a magnetic stirrer, a reflux condenser, a Dean−Stark trap, a nitrogen inlet and outlet, 3,5-dichlorobenzenethiol (1.0 g, 5.59 mmol) as an AB_2 monomer for hyperbranched poly(phenylene sulfide) (HPPS), sodium carbonate (1.2 g, 11.3 mmol), toluene (20 mL), and *N*-methyl-2-pyrrolidinone (10 mL) were charged. The mixture was then heated to 160 °C. The water generated during the reaction was removed by azeotropic distillation with toluene. After 4−5 h, dehydration was completed. The mixture was further stirred at this temperature for additional 6 h and poured into 500 mL of distilled water containing 50 mL of conc. hydrochloric acid. The precipitates were washed with water and collected by suction filtration. The resultant solids were transferred to an extraction thimble and Soxhlet-extracted with water for three days and methanol for three more days, and finally freeze-dried for 48 h to give 0.73 g (91.3% yield) of HPPS as a brown powder. Anal. Calcd for C_6H_3SCl: C, 50.53; H, 2.12. Found: C, 50.95; H, 2.14.

The polymerization of the 4-chlorobenzenethiol (2.0 g, 13.8 mmol) as an AB monomer for linear poly(phenylene sulfide) (LPPS) was conducted following the same procedure used for 3,5-dichlorobenzenethiol. After complete workup of the isolated polymer, the yield was 55.3%. Anal. Calcd for C_6H_4S: C, 66.63; H, 3.73. Found: C, 64.18; H, 3.59.

Representative in Situ Polymerization of 3,5-Dichlorobenzenethiol with 10 wt % of CB-MWNT Load (HPPS-*g*-MWNT). In the same reaction setup for the synthesis of HPPS, 3,5-dichlorobenzenethiol (4.5 g, 25.1 mmol), CB-MWNT (0.5 g), sodium carbonate (6.0 g, 56.6 mmol), toluene (100 mL), and *N*-methyl-2-pyrrolidinone (50 mL) were charged. Following the same reaction and workup procedures described for HPPS, the yield was almost quantitative to give 4.04 g (99.0% yield) of the product as a gray powder. Anal. Calcd for $C_{7.61}H_{3.04}SCl$: C, 56.38; H, 1.89. Found: C, 56.40; H, 1.80.

The *in situ* polymerization of the 4-chlorobenzenethiol (2.7 g, 18.7 mmol) in the presence of CB-MWNT (0.3 g) to generate LPPS-*g*-MWNT followed the same procedure used for the synthesis of HPPS-*g*-MWNT. After complete workup procedure, the yield was 59.2%. Anal. Calcd for $C_{7.30}H_{4.03}O_{0.01}S$: C, 70.75; H, 3.28. Found: C, 71.24; H, 2.82.

Blends of CB-MWNT with LPPS or HPPS. CB-MWNT (0.010 g) was blended with LPPS (0.036 g) in THF. CB-MWNT, LPPS and tetrahydrofuran (THF, l mL) were placed in a 5 mL vial. The vial was sealed and stirred with magnetic stirrer. After 24 h stirring at room temperature, THF was evaporated to dryness. The black residues were freeze-dried for 48 h to give CB-MWNT/LPPS blend. Similarly, CB-MWNT/HPPS blend was also prepared by adding CB-MWNT (0.010 g) and HPPS (0.072 g) in THF.

Results and Discussion

The functionalization of MWNT was carried out with 4-chlorobenzoic acid in PPA/P_2O_5 medium at 130 °C (Scheme 1a). The resultant CB-MWNT were covalently bonded with 4-chlorobenzoyl moieties, which could be useful sites for the introduction of various functionalities via nucleophilic substitution reaction. To elucidate the reaction between activated aromatic chloride and aromatic thiol, model reaction of CB-MWNT were carried out in NMP in the presence of sodium carbonate (Scheme 1b). In this research, conductive LPPS and HPPS were grafted onto the sites activated by carbonyl group in NMP/toluene in the presence of sodium carbonate at 160 °C (Scheme 2, parts a and b). LPPS is commercially available, has excellent chemical and thermal stability, can be melt-processed readily into films and fibers, and is the precursor to a conducting polymer of the semiflexible rod polymer family.[21] Thus, the resultant nanocomposites, LPPS-*g*-MWNT and HPPS-*g*-

Scheme 1. (a) Functionlization of MWNT in Polyphosphoric Acid/Phorous Pentoxide and (b) Model Reaction of CB-MWNT and 4-Methylbenzenethiol in NMP/Toluene in the Presence of Sodium Carbonate

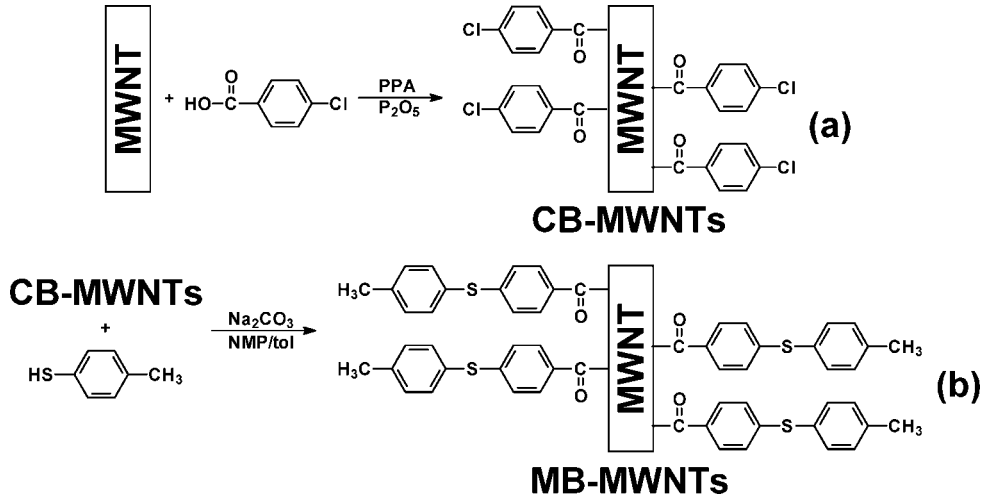

Scheme 2. Grafting of (a) LPPS and (b) HPPS onto CB-MWNT and (c) Synthesis of LPPS and HPPS

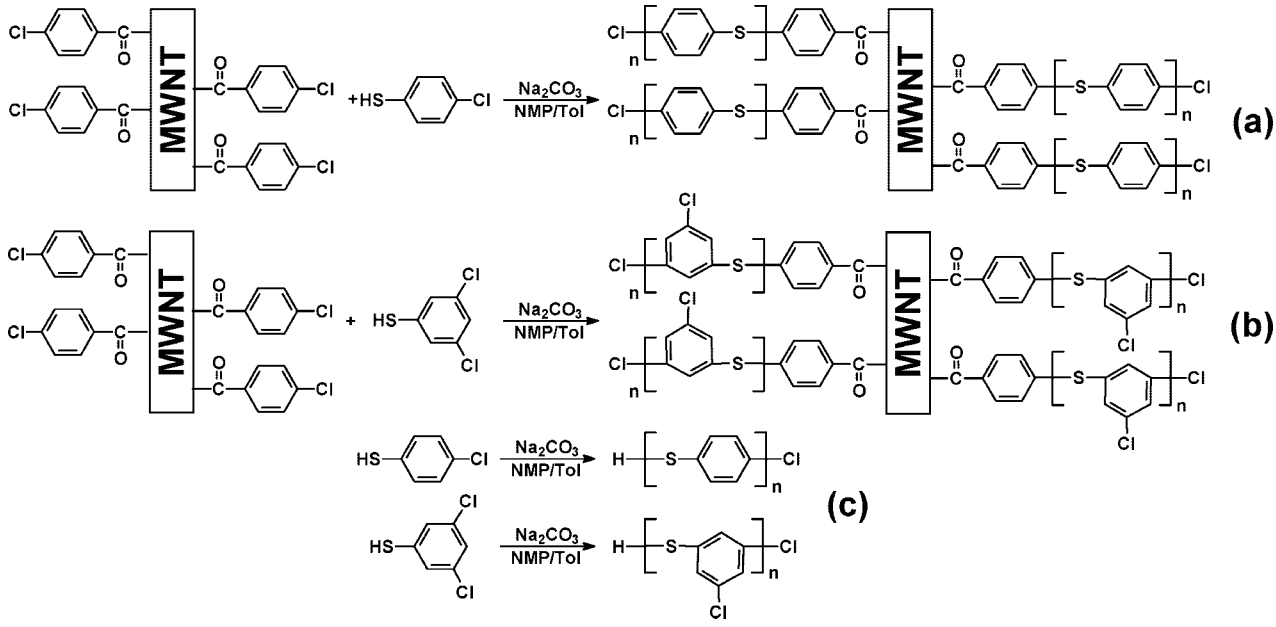

MWNT, are expected to display enhanced conductivities and could be fabricated from both solution and melt states.

FT-IR Study. The FT-IR spectroscopy was used as a convenient and informative analytical tool to monitor the progress of functionalization, polymerization, and grafting processes. To eliminate potential impurities, all samples were completely worked-up in the Soxhlet extraction in water for three days to remove any residual solvents and in methanol for three additional days to get rid of low molar mass impurities before they were characterized. The existence of sp^2 C−H and sp^3 C−H stretching bands around 2969 cm^{-1}, which could be attributed by the defects at sidewalls and open ends of MWNT, was previously reported.[12] These defects were originated during the synthetic process of MWNT based on hydrocarbon feedstock.[22] They were the primary sites for the electrophilic substitution reactions. To afford 4-chlorobenzoyl functionalized MWNT (CB-MWNT), "direct" Friedel−Crafts acylation reaction between MWNT and 4-chlorobenzoic acid was carried out in PPA/P_2O_5 medium.[23] The resultant CB-MWNT displayed characteristic C═O stretching band at 1642 cm^{-1} (Figure 1a). The result confirmed that MWNT had been successfully functionalized to form CB-MWNT.

The model compound MB-MWNT displayed stronger intensities of sp^2 C−H and sp^3 C−H peaks centered at 2922 and 2850 cm^{-1}, respectively (Figure 1a). In addition, carbonyl stretching peak was shifted to a lower wavenumber at 1636 cm^{-1}, compared to the peak at 1642 cm^{-1} of CB-MWNT, due to the electron-donating effect of *para*-thioether group in MB-MWNT that increases electron density of the carbon of C═O bond. The substitution effect has clearly lengthened the C═O bond slightly. These results supported the expectation that the aromatic-nucleophilic-substitution model reaction between CB-MWNT and 4-methylbenzenethiol was successful. Other supportive data are presented in following sections.

For comparison purposes, the FT-IR spectra of the pristine MWNT, homopolymers, and monomers are depicted in Figure 1. The S−H stretches around 2570−2575 cm^{-1} and C−S stretches around 800−818 cm^{-1} for the starting monomers are respectively presented in the 4-chlorobenzenethiol (4-CBT) and 3,5-dichlorobenzenethiol (3,5-DCBT) spectra (Figure 1b and 1c). Both LPPS and LPPS-*g*-MWNT samples sulfide (C−S) dis-

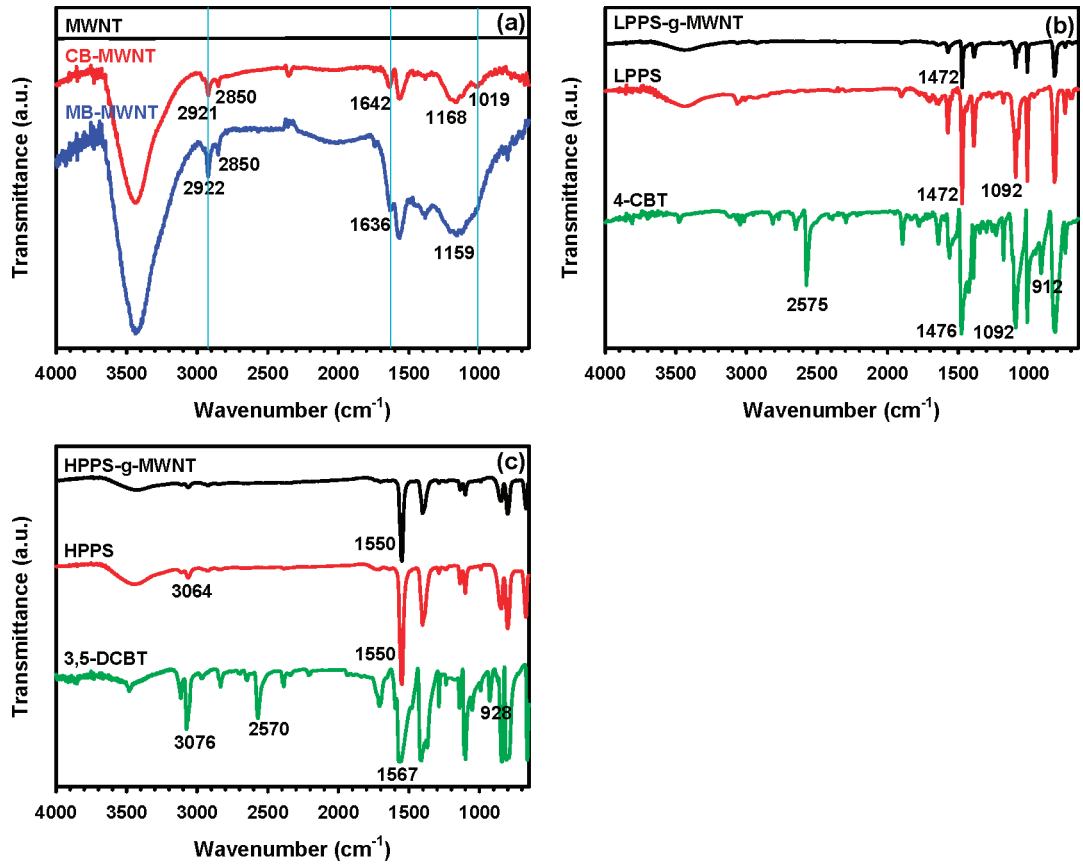

Figure 1. FT-IR (KBr pellet) spectra of samples: (a) MWNT, CB-MWNT and MB-MWNT; (b) 4-CBT, LPPS, LPPS-*g*-MWNT; (c) 3,5-DCBT, HPPS, HPPS-*g*-MWNT.

played peaks at 818 cm^{-1}. However, there was no detectable thiol (S−H) peak at 2575 cm^{-1} in reference to the 4-CBT monomer (Figure 1b). Similarly, in HPPS and HPPS-*g*-MWNT samples, the sulfide (C−S) bond displayed peaks around 800 cm^{-1} and there was also no thiol (S−H) peak at 2570 cm^{-1} as compared to the 3,5-DCBT monomer (Figure 1c). Thus, LPPS and HPPS would have been grafted to the surface of CB-MWNT to afford LPPS-*g*-MWNT and HPPS-*g*-MWNT, respectively. To estimate the amount of free LPPS and HPPS, specific amounts of LPPS-*g*-MWNT and HPPS-*g*-MWNT were Soxhlet extracted with THF for 24 h. Their weight losses after Soxhlet extraction and dry were less than 2−3%. This result implies that there exist almost no LPPS and HPPS homopolymers in the LPPS-*g*-MWNT and HPPS-*g*-MWNT nanocomposites, respectively. Clearly, the photographs of the samples displayed gray color instead of dark black color due to CB-MWNT (Figure S1, Supporting Information), which would indirectly mean that the polymers are uniformly grafted and CB-MWNT are completely wrapped.

Solubility. For the reference, LPPS and HPPS homopolymers were also synthesized via aromatic nucleophilic substitution reaction from self-polymerizable AB or AB_2 monomer as described in Scheme 2c. LPPS is commercially prepared by the reaction between 1,4-dichlorobenzene and sodium sulfide.[24] The LPPS sample in this study was prepared from 4-chlorobenzenethiol. It is soluble in strong acids such as sulfuric acid, methanesulfonic acid (MSA), and trifluoroacetic acid (TFAc). For nonacidic solvents, it is soluble in polar aprotic solvents such as *N*,*N*-dimethylformamide (DMF), *N*,*N*-dimethylacetamide (DMAc), dimethyl sulfoxide (DMSO), *N*-methyl-2-pyrrolidinone (NMP), and carbon disulfide (CS_2). It is also soluble in one of ether solvents, viz. THF. Interestingly, HPPS homopolymer is soluble in THF and CS_2, but it was marginally soluble in polar aprotic solvents such as NMP, DMAc, DMF, DMSO, etc. In general, hyperbranched polymers are known to display better solubility than their linear analogs,[25] and the unexpected solubility behavior of HPPS is due significantly to the large number of chlorine groups on its periphery. Deductively, HPPS is indeed soluble in common chlorinated solvents such as dichloromethane, chloroform, carbon tetrachloride, chlorobenzene, and 1,2-dichlorobenzene. However, CB-MWNT formed a stable dispersion in THF, dichloromethane, or carbon tetrachloride. Although the nanocomposite samples, LPPS-*g*-MWNT and HPPS-*g*-MWNT, were not completely soluble in any of above-mentioned solvents, the solution colors of LPPS-*g*-MWNT and HPPS-*g*-MWNT turned dark, indicating that small portions of the samples were dispersed into those solvents.

Scanning Electron Microscopy (SEM). The SEM images presented in Figure 2 are taken for the pristine MWNT and as-prepared samples. The pristine MWNT image shows that the tubes have seamless and smooth surfaces. The average diameter of pristine MWNT is 10−20 nm (Figure 2a). At the same magnification, however, the average diameter of CB-MWNT is approximately 40 nm, which is 2−4 times thicker than that of pristine MWNT (Figure 2b). Interestingly, the shape of tube could be discerned by two parts. Opaque inner-hard core is covered by translucent outer-shadow-like part (Figure 2b, arrow). The diameter dimension (10−20 nm) of inner-hard core corresponds well to that of the parent MWNT. Outer-shadow-like part could be due to the 4-chlorobenzoyl moieties that have uniformly covered the surface of CB-MWNT. The SEM image of LPPS-*g*-MWNT reveals that the diameter approaches 100 nm (Figure 2c). This value is much larger than pristine MWNT (10−20 nm) and CB-MWNT (~40 nm). Thus, it is an indication that LPPS is heavily grafted to the CB-MWNTs. In the case of HPPS-*g*-MWNT, although the diameter dimension is close to

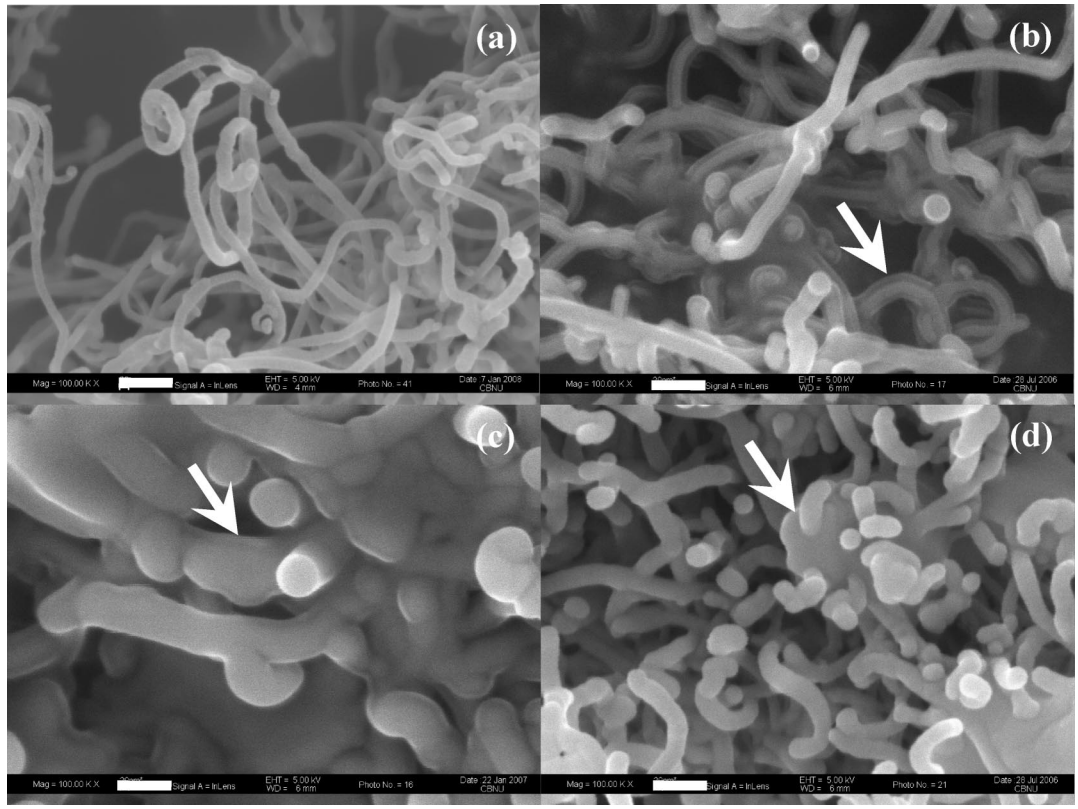

Figure 2. SEM images of as prepared samples: (a) as-received MWNT (100 000×); (b) as-prepared CB-MWNT (100 000×); (c) as-prepared LPPS-*g*-MWNT (100 000×); (d) as-prepared HPPS-*g*-MWNT (100 000×). Scale bars are 100 nm.

that of CB-MWNT, the original outer-shadow-like part of CB-MWNT (see Figure 2b) appears to be completely covered with HPPS (Figure 2d). Moreover, some locations are clearly filled with big chunk of HPPS (Figure 2d, arrow). The tube ends of the samples CB-MWNT, LPPS-*g*-MWNT, and HPPS-*g*-MWNT are heavily sealed with organics and they are spherical in shape. Owing to the larger population of sp^2 C−H and the greater bond strain (surface curvature) at the ends of tubes, the larger number of reactive sites is available at the tube ends.[15] Although the 4-chlorobenzoyl moieties are uniformly attached to MWNT (Figure 2b), the density of CB-MWNT outer layer is much lower than those of LPPS-*g*-MWNT and HPPS-*g*-MWNT (Figure 2c and 2d). It could be confirmed that polymers were more densely covering the outer layers of CB-MWNT.

To further emphasize the surface morphology difference between CB-MWNT and MB-MWNT, SEM image of MB-MWNT is presented in Figure 3a. Probably because of the methyl groups on the outermost part of MB-MWNT, the surface appears fluffy. The 5% weight loss of MB-MWNT in air occurred at 502 °C (Figure 3b), which was approximately 69 °C lower than that of CB-MWNT (571 °C). This result also indirectly implies that the polymers were presumably grafted onto the surfaced CB-MWNT. However, these observations are insufficient to rule out the possibility that the LPPS and HPPS could physically wrap around CB-MWNT. Thus, the physical blends of LPPS/CB-MWNT and HPPS/CB-MWNT were prepared. The SEM images clearly show the difference between the polymer-grafted MWNT samples (Figure 2c and 2d) and their corresponding blends. The CB-MWNT, whose diameter remained practically the same, clearly aggregated in LPPS or HPPS matrix (Figure 3c and 3d). Therefore, we conclude that the LPPS and HPPS polymers have been grafted onto the surface of CB-MWNT in LPPS-*g*-MWNT and HPPS-*g*-MWNT, respectively.

To present visual evidence of the natures of LPPS and HPPS on the surface of MWNT, LPPS-*g*-MWNT and HPPS-*g*-MWNT were compression molded into sheets at 250 and 300 °C, respectively. The SEM images of the fracture surfaces of the samples displayed completely different morphologies compared to as-prepared samples, which were not heat treated (see Figure 2). In the case of LPPS-*g*-MWNT sample, LPPS crystals are uniformly attached to the surface of MWNT with approximately 40 nm of diameter dimension (Figure 4a). Since LPPS is a semicrystalline polymer, its grafts must have been crystallized by annealing during the process of compression molding. The zoomed-in image shows that there is no discernible boundary between MWNT and LPPS (Figure 4a, inset). This is because upon crystallization, the electron density of LPPS must be sufficiently high to render distinguishing it from MWNT difficult. On the other hand, the SEM image of HPPS-*g*-MWNT displays relatively smooth surface morphology. MWNT are intermingled by molten HPPS (Figure 4b), which is expected to be an amorphous polymer, whose electron density compared to semicrystalline analog is lower and thus the boundary between MWNT and HPPS can be clearly discernible (Figure 4b, inset).

Transmission Electron Microscopy (TEM). To visually tell whether the basic structure of MWNT remaining intact during the reaction sequence, and verify the covalent attachment of the respective polymers, LPPS-*g*-MWNT and HPPS-*g*-MWNT were dispersed in MSA and the mixture was diluted with large amount of NMP. The carbon coated grid was dipped into the mixture and taken out to dry in a vacuum oven. The TEM images of LPPS-*g*-MWNT and HPPS-*g*-MWNT show that the tubes are heavily decorated with polymers (Figure 5, parts a and b). Furthermore, the clear wall-to-wall stripes of MWNT framework at high magnification (see Figure S2, Supporting Information) suggest that the structural stability of MWNT under the reaction conditions in a mildly

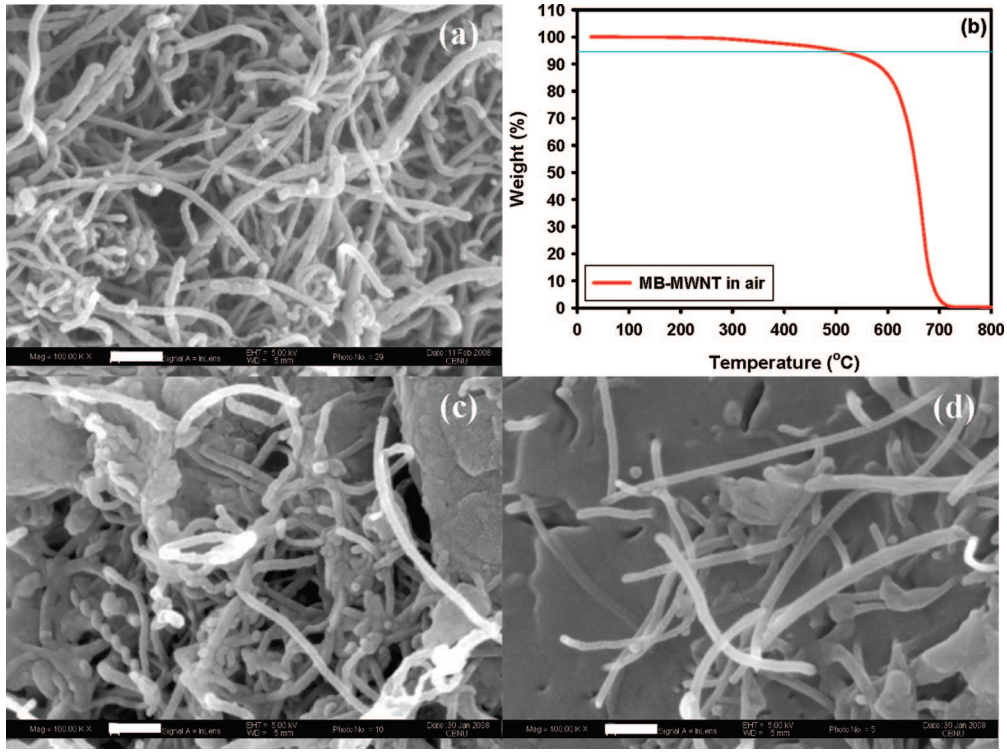

Figure 3. (a) SEM image of as-prepared MB-MWNT (100 000×); (b) TGA thermogram MB-MWNT in air with heating rate of 10 °C/min; (c) as-prepared LPPS/CB-MWNT blend (100 000×); (b) as-prepared HPPS/CB-MWNT blend (100 000×). Scale bars are 100 nm.

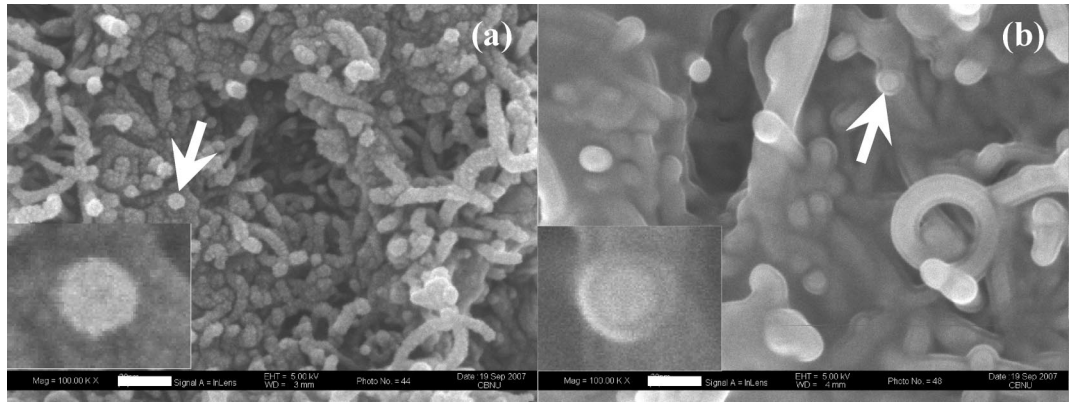

Figure 4. SEM images obtained from the fracture surfaces of compression molded samples: (a) LPPS-*g*-F-MWNT (100 000×); (b) HPPS-*g*-F-MWNT (100 000×). Scale bars are 100 nm.

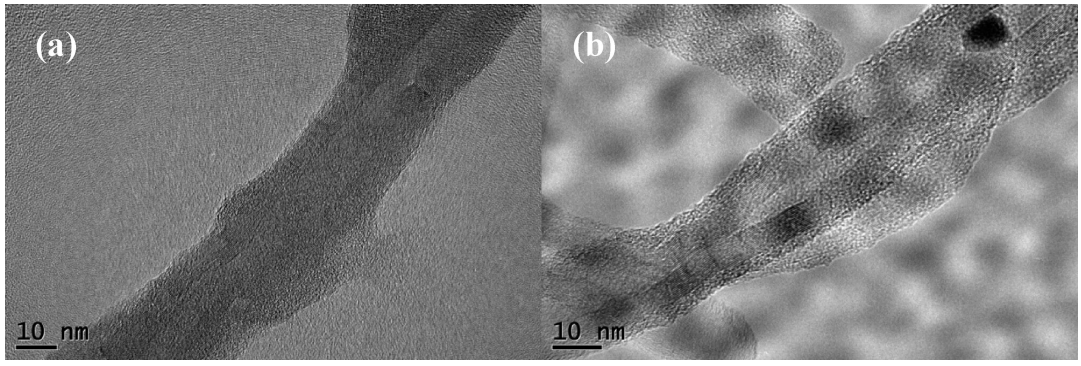

Figure 5. TEM images of samples: (a) LPPS-*g*-MWNT; (b) HPPS-*g*-MWNT.

acidic medium, PPA/P_2O_5, for the functionalization to afford CB-MWNT via electrophilic substitution reaction and in a mildly basic medium NMP/Na_2CO_3 for graft-polymerization to afford PPS-*g*-MWNT via a nucleophilic substitution reaction. In addition to both reaction sequences, MWNT framework maintained its structural integrity throughout complete workup procedures at each reaction step. The unique combination of microscopic results explains that the processes applied in this

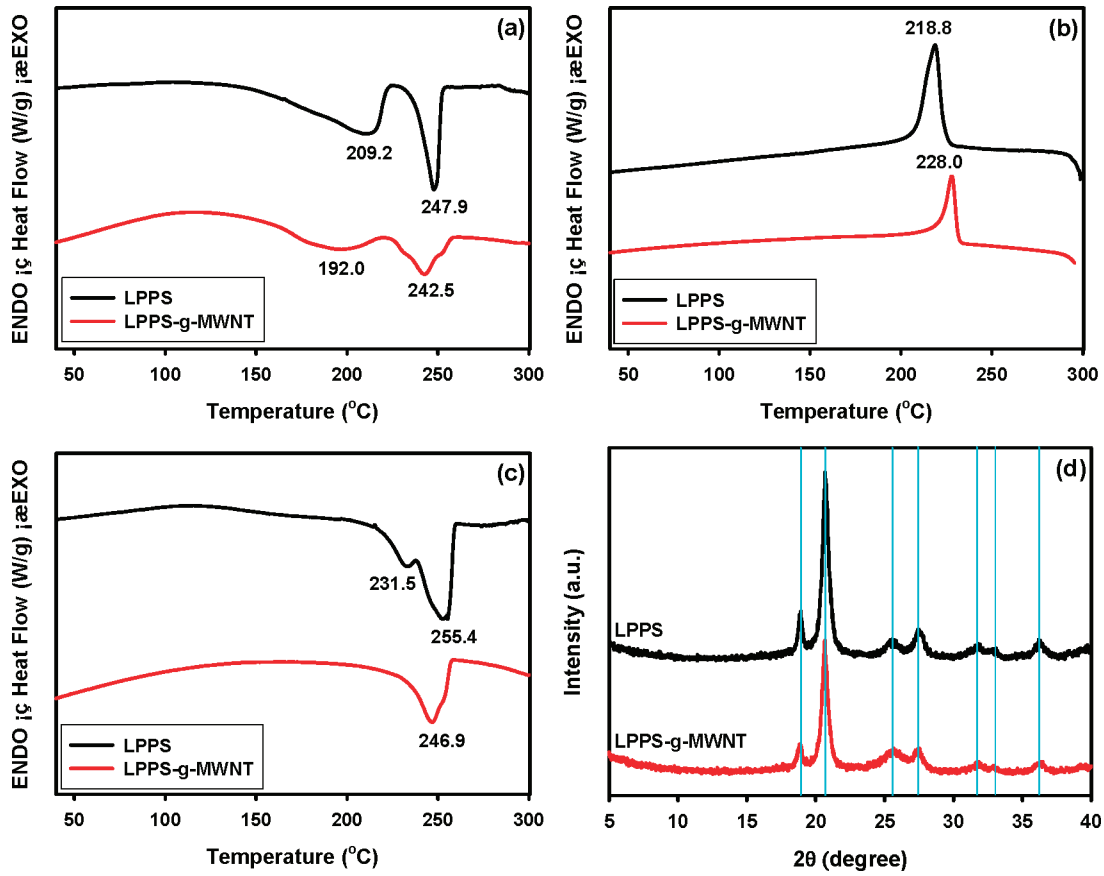

Figure 6. DSC thermograms of nanocomposites obtained with heating rate of 10 °C/min: (a) first heating scan; (b) first cooling scan; (c) second heating scan; (d) X-ray diffraction patterns.

Table 1. Thermal Properties of Homopolymers and Nanocomposites

	DSC[a]					TGA[b]			
						in air at 800 °C		in N_2 at 800 °C	
sample	T_g (°C)	T_c (°C)	ΔH_c (J/g)	T_m (°C)	ΔH_f (J/g)	$T_{d5\%}$ (°C)	char (%)	$T_{d5\%}$ (°C)	char (%)
LPPS		218.8	50.6	247.9 (255.4)	27.0 (23.0)	371	~0	366	40
LPPS-*g*-MWNT		228.0	33.7	242.5 (246.9)	21.0 (31.6)	376	~0	367	56
HPPS	74.6					451	~0	490	44
HPPS-*g*-MWNT	79.7			305.7		420	~0	471	49

[a] Glass transition temperature (T_{gh}), crystallization temperature (T_c), and melting temperature (T_m) determined by DSC with heating and cooling rates both at 10 °C/min. The number in the parentheses are melting temperature (T_m) determined from the second heating run with a heating rate of 10 °C/min. [b] The temperature at which 5% weight loss occurred during TGA scan obtained with a heating rate of 10 °C/min.

work are indeed viable for the functionalization and grafting of MWNT.

Thermal Properties. The transition temperatures of the homopolymers and nanocomposites were determined by differential scanning calorimetry (DSC). The powder samples were subjected to two cycles of heating from room temperature to 300 or 350 °C, and then cooling to 20 °C with a ramping rate of 10 °C/min. The glass transition temperature (T_g) was taken as the midpoint of the maximum baseline shift from the each run. As shown in Figure 6a and Table 1, LPPS homopolymer is a semicrystalline material with two endothermic transition temperatures at 209 and 248 °C. The appearance of multiple morphologies for LPPS with respect to thermal history (i.e., before annealing) has been reported.[26] Its recrystallization temperature after melting is 219 °C during the cooling scan (Figure 6b). At the second heating scan, the separation of melting endotherms is narrowed considerably, and the peaks are centered at 232 and 255 °C (Figure 6c). In the case of LPPS-*g*-MWNT, the melting endotherms are present at 192 and 242.5 °C during the first heating scan (Figure 6a). The lower temperatures for the endotherms of LPPS-*g*-MWNT compared to those for LPPS could be attributed by smaller and less stable LPPS crystals in the nanocomposite than in the neat polymer. The fact that LPPS-*g*-MWNT displays higher recrystallization temperature at 228 °C than LPPS at 219 °C can be a possible explanation for lower melting temperatures observed. Since MWNT is acting as a nucleation agent for LPPS, fast crystallization rate results in smaller and less stable crystals in the system. The double melting endotherms of LPPS-*g*-MWNT occurred in the first heating scan is more closely merged into a single endotherm at 247 °C in the second heating scan, which is approximately 8.5 °C lower than that of LPPS (Figure 6c). The result also confirms the role of MWNT as a nucleation agent in the LPPS matrix. The X-ray diffraction patterns of LPPS and LPPS-*g*-MWNT are almost identical (Figure 6d). The *d*-spacing values are 2.48, 2.82, 3.24, 3.49, 4.29, and 4.70 Å. The only difference between these samples is the peak intensity for the interplane $\pi-\pi$ distance at 3.49 Å. Due to the overlapping of diffraction intensities associated with the wall-to-wall distance of MWNT and the interplane $\pi-\pi$ distance of PPS, this peak intensity is stronger for LPPS-*g*-MWNT than the LPPS homopolymer.

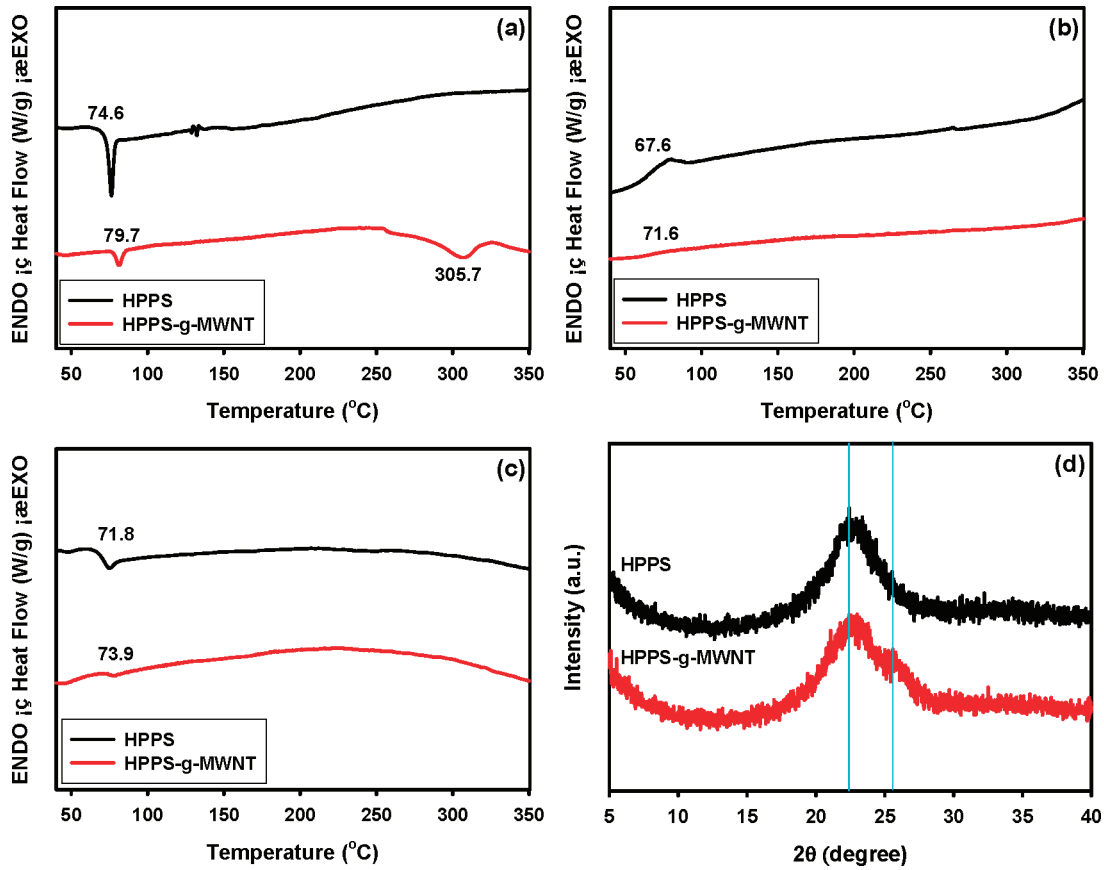

Figure 7. DSC thermograms of nanocomposites obtained with heating rate of 10 °C/min: (a) first heating scan; (b) first cooling scan; (c) second heating scan; (d) X-ray diffraction patterns.

As hyperbranched polymers are generally known to be amorphous materials,[27] the T_g of HPPS was at 74.6 °C with a strong hysteresis in the first heating scan (Figure 7a). The values obtained from the cooling and second heating scans were 67.6, and 71.8 °C, respectively. Since the graft is an amorphous material, the sample HPPS-*g*-MWNT is also expected to display only T_g and it is found at 79.7 °C, approximately 5 °C higher than that of the HPPS homopolymer. However, there is a weak endothermic melting peak at 305.7 °C in the first heating scan. It is believed that CB-MWNT must have acted as a nucleation agent for HPPS to form crystals. The crystal melting peak disappears in the second heating scan. This is a strong indication that HPPS and CB-MWNT are intimately interacting with each other. Therefore, it is reasonable that HPPS are presumably grafted onto CB-MWNT. Those peaks disappear in the cooling scan (Figure 7b) and the second heating scan (Figure 7c), due to the rate of crystallization is too slow. In general, the T_g of the matrix polymer in a nanocomposite is increased proportionate to the MWNT content when MWNTs are homogeneously incorporated, because they act as rigid fillers. Therefore, the T_g's of HPPS-*g*-MWNT are 2−5 °C higher than those of HPPS homopolymer in the all scans. The XRD pattern can further validate that HPPS is indeed an amorphous material, which displays dark hollow XRD patterns without crystal peaks (Figure 7d). The sample HPPS-*g*-MWNT displays a shoulder peak at $2\theta = 25.92°$, which translates to a *d*-spacing value of 3.43 Å > for the wall-to-wall distance of MWNT.

The polymers and nanocomposites (powder samples) were subjected to thermogravimetric analysis (TGA) in both air and nitrogen to evaluate their thermo-oxidative stability and thermal stability, respectively. The results are presented in Figure 8 and summarized in Table 1. LPPS and HPPS indicated that temperature at which 5% weight loss ($T_{d5\%}$) in air occurred at 371 and 451 °C and in nitrogen at 366 and 490 °C, respectively (Figure 8, parts a and b). The char yields of both LPPS and HPPS homopolymers in air at 800 °C were approximately 0%. Their char yields in nitrogen at 800 °C were 40 and 44%, respectively. The $T_{d5\%}$ values for CB-MWNT, LPPS-*g*-MWNT and HPPS-*g*-MWNT in air were 571, 376, and 420 °C in that order (Figure 8a). The values in nitrogen were at 770, 367, and 471 °C (Figure 8b) in that order. The char yields of nanocomposites in air at 800 °C were also ∼0%. The values of CB-MWNT, LPPS-*g*-MWNT and HPPS-*g*-MWNT in nitrogen at 800 °C were 94, 56, and 49% in that order. LPPS-*g*-MWNT displayed a thermo-oxidative stability approximately 5 °C higher than that of LPPS homopolymer, while HPPS-*g*-MWNT was approximately 31 °C lower than that of HPPS homopolymer. Besides, changes of inclination are in LPPS-*g*-MWNT at about 500 °C and in HPPS-*g*-MWNT at about 550 °C. It could be another strong indication that polymers are attached to the surface of CB-MWNT to LPPS-*g*-MWNT and HPPS-*g*-MWNT nanocomposites. Moreover, stepwise weight loss of LPPS, HPPS, LPPS-*g*-MWNT, and HPPS-*g*-MWNT samples corroborates the DSC result that samples are in the multiple forms (Figure 8a).

The samples were also subjected to an isothermal oxidative stability experiment. The powder samples were placed in the heating chamber under air atmosphere and at 320 °C for 10 h. The results are shown in Figure 8c. At any given time during this period, the HPPS and HPPS-*g*-MWNT was more resistant to thermo-oxidative degradation than LPPS and LPPS-*g*-MWNT. Isothermal aging curves of HPPS and HPPS-*g*-MWNT in air reveal that both have almost identical thermo-oxidatve resistance, and both samples retained more than 97% of their original weights up to 10 h. In the cases of LPPS and LPPS-*g*-MWNT, the samples started to lose their weights very rapidly from the

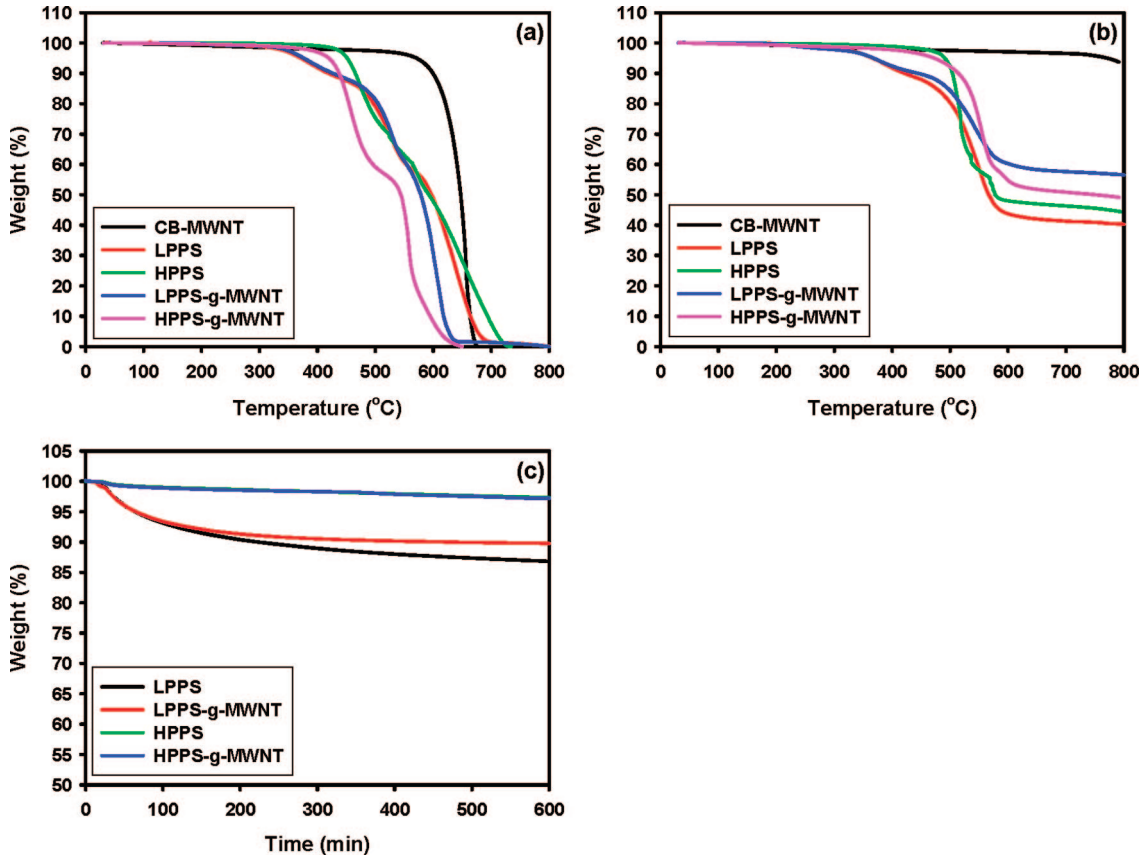

Figure 8. TGA thermograms of nanocomposites: (a) in air with heating rate of 10 °C/min; (b) in nitrogen with heating rate of 10 °C/min; (c) isothermal thermooxidative stability experiment at 320 °C in air.

beginning to 200 min. After 10 h at 320 °C in air, they retained approximately 87 and 90% of their original weights, respectively.

Conductivity Measurements. LPPS-*g*-MWNT and HPPS-*g*-MWNT nanocomposites were compression molded at 250 and 300 °C, respectively. The electrical resistivities of LPPS-*g*-MWNT and HPPS-*g*-MWNT were measured by a digital nanovoltmeter instrument. Each specimen was measured 10 times at different locations and the average values were reported. The measured resistance values without doping were 0.085 and 0.28 Ωcm, respectively. The conductivity of those was determined by the following equation $\sigma = 1/(\rho \times \mathrm{cf} \times d)$, where σ, ρ, cf (4.1544), and d are the conductivity, the resistivity, correction factor, and sample thickness, respectively.[28] The calculated conductivities of the LPPS-*g*-MWNT and HPPS-*g*-MWNT were 11.76 and 3.56 S/cm, respectively. The values for blended samples, LPPS/CB-MWNT and HPPS/CB-MWNT, were out of detection limit (10^{-6} S/cm). LPPS/expanded graphite and LPPS/ultrasonicatedly expanded graphite nanocomposites prepared by melt blending displayed their conductivities in the range $10^{-2}-10^{-3}$ S/cm when the nanocomposites contained 10 wt % of expanded graphite.[13] The values LPPS-*g*-MWNT and HPPS-*g*-MWNT namocomposites were improved 2−4 orders of magnitude compared to the literature report.[13] The good electrical conductivity of LPPS-*g*-MWNT and HPPS-*g*-MWNT implies that the basic structure of CB-MWNT was minimally damaged, if any, during the fuctionalization process. Thus, CB-MWNTs in the LPPS and HPPS matrices were completely exfoliated to provide maximum aspect ratio. Between the samples, LPPS-*g*-MWNT nanocomposites had higher conductivity than HPPS-*g*-MWNT nanocomposites mostly likely because of *para*-conjugated structure of LPPS.

Conclusion

The LPPS-*g*-MWNT and HPPS-*g*-MWNT nanocomposites were successfully prepared by two-step reaction sequences in PPA/P_2O_5 mixture via an electrophilic substitution reaction and NMP/toluene in the presence of sodium carbonate via a nucleophilic substitution reaction. The structures and properties of resultant nanocomposites were characterized with FT-IR, SEM, TEM, and TGA. On the basis of these combined results, we believe that most of the LPPS and HPPS were covalently grafted onto the surface of CB-MWNT and thus both reactions are indeed useful for hybridization of carbon nanomaterials and conductive polymer precursors to expect synergetic enhancements that could be originated from the specific attribute of each component. Toward an important objective for the development of multifunctional carbon-based nanocomposites, i.e., the minimization of conductivity loss upon functionalization of CNTs, apart from having high thermal stability, the nanocomposites prepared in this study also exhibited good electrical conductivity at 11.76 and 3.56 S/cm.

Acknowledgment. We are grateful to Jeong Hee Lee of Chungbuk National University for conducting SEM. This project was supported by funding from US Air Force Office of Scientific Research, Asian Office of Aerospace R&D (AFOSR-AOARD) and Korea Science and Engineering Foundation (R01-2007-000-10031-01).

Supporting Information Available: Figure S1 showing color photographs of as-prepared powder samples (a) LPPS-*g*-MWNT and (b) HPPS-*g*-MWNT, where the gray color instead of dark black of the nanocomposite samples implies that the polymers are uniformly grafted and CB-MWNT is completely covered, and Figure S2, showing TEM images of samples at high magnification,

(a) LPPS-*g*-MWNT and (b) HPPS-*g*-MWNT, where clear stripes at high magnification indicate that MWNT frameworks are structurally intact during the reactions and workup procedures. This material is available free of charge via the Internet at http://pubs.acs.org.

References and Notes

(1) (a) Andrews, R.; Jacques, D.; Rao, A. M.; Rantell, T.; Derbyshire, F.; Chen, Y.; Haddon, R. C. *Appl. Phys. Lett.* **1999**, *75*, 1329. (b) Qian, D.; Dickey, E. C.; rews, R.; Rantell, T. *Appl. Phys. Lett.* **2000**, *76*, 2868. (c) Shaffer, M. S. P.; Windle, A. H. *Adv. Mater.* **1999**, *11*, 937. (d) Zin, L.; Bower, C.; Zhou, O. *Appl. Phys. Lett.* **1998**, *73*, 1197. (e) Haggenmueller, R.; Gommans, H. H.; Rinzler, A. G.; Fischer, J. E.; Winey, K. I. *Chem. Phys. Lett.* **2000**, *330*, 219. (f) Chen, G. Z.; Shaffer, M. S. P.; Coleby, D.; Dixon, D.; Zhou, W.; Fray, D. J.; Windle, A. H. *Adv. Mater.* **2000**, *12*, 522. (g) Sandler, J.; Shaffer, M. S. P.; Prasse, T.; Bauhofer, W.; Schulte, K.; Windle, A. H. *Polymer* **1999**, *40*, 5967. (h) Part, C.; Ounaies, Z.; Watson, K. A.; Crooks, R. E.; Smith Jr., J.; Lowther, S. E.; Connell, J. W.; Siochi, E. J.; Harrison, J. S.; St. Clair, T. L. *Chem. Phys. Lett.* **2002**, *364*, 303.

(2) Ounaies, Z.; Park, C.; Wise, K. E.; Siochi, E. J.; Harrison, J. S. *Compos. Sci. Technol.* **2003**, *63*, 1637.

(3) McLachlan, D. S.; Chiteme, C.; Park, C.; Wise, K. E.; Lowther, S. E.; Lillehei, P. T.; Harrison, J. S. *J. Polym. Sci., Part B: Polym Phys.* **2005**, *43*, 3273.

(4) Barrau, S.; Demont, P.; Peigney, A.; Laurent, C.; Lacabanne, C. *Macromolecules* **2003**, *36*, 5187.

(5) Jiang, X.; Bin, Y.; Matsou, M. *Polymer* **2005**, *46*, 7418–7424.

(6) Sandler, J. K. W.; Kirk, J. E.; Kinloch, I. A.; Shaffer, M. S. P.; Windle, A. H. *Polymer* **2003**, *44*, 5893.

(7) Du, F.; Scogna, R. C.; Zhou, W.; Brand, S.; Fischer, J. E.; Winey, K. I. *Macromolecules* **2004**, *37*, 9048.

(8) Song, Y. S.; Youn, J. R. *Carbon* **2005**, *43*, 1378.

(9) Ajayan, P. M.; Schadler, L. S.; Giannaris, C.; Rubio, A. *Adv. Mater.* **2000**, *12*, 750.

(10) (a) Monthioux, M.; Smith, B. W.; Burteaux, B.; Claye, A.; Fischer, J. E.; Luzzi, D. E. *Carbon* **2001**, *39* (8), 1251. (b) Zhang, T.; Shi, Z.; Gu, Z.; Iijima, S. *Carbon* **2000**, *38*, 2055.

(11) Salzmann, C. G.; Llewellyn, S. A.; Tobias, G.; Ward, M. A. H.; Huh, Y.; Green, M. L. H. *Adv. Mater.* **2007**, *19* (6), 883.

(12) Heller, D. A.; Barone, P. W.; Strano, M. S. *Carbon* **2005**, *43*, 651.

(13) Huang, W.; Lin, Y.; Taylor, S.; Gaillard, J.; Rao, A. M.; Sun, Y. P. *Nano Lett.* **2002**, *2*, 231.

(14) Sammaliorpi., M; Krasheninnikow., A.; Kuronen., A.; Nordlund., K.; Kaski., K. *Phys. Rev. B.* **2004**, *70*, 7.

(15) (a) Baek, J.-B.; Lyon, C. B.; Tan, L.-S. *J. Mater. Chem.* **2004**, *14*, 2052. (b) Baek, J.-B.; Lyons, C. B.; Tan, L.-S. *Macromolecules* **2004**, *37*, 8278. (c) Lee, H.-J.; Oh, S.-J.; Choi, J.-Y.; Kim, J. W.; Han, J.; Tan, L.-S.; Baek, J.-B. *Chem. Mater.* **2005**, *17*, 5057. (d) Oh, S.-J.; Lee, H.-J.; Keum, D.-K.; Lee, S.-W.; Park, S.-Y.; Tan, L.-S.; Baek, J.-B. *Polymer* **2006**, *47*, 1132. (e) Choi, J.-Y.; Oh, S.-J.; Lee, H.-J.; Wang, D. H.; Tan, L.-S.; Baek, J.-B. *Macromolecules* **2007**, *40*, 4474. (f) Choi, J.-Y.; Huh, W; Tan, L.-S.; Baek, J.-B. *Polymer* **2007**, *48*, 4034. (g) Wang, D. H.; Arlen, M. J.; Baek, J.-B.; Vaia, R. A.; Tan, L.-S. *Macromolecules* **2007**, *40*, 6100.

(16) Yang, J.; Xu, T.; Lu, A.; Zhang, Q.; Fu, Q J. *Appl. Polym. Sci.* **2008**, *109*, 720.

(17) (a) Zhao, Y. F.; Xiao, M.; Wang, S. J.; Ge, X. C.; Meng, Y. Z. *Comp. Sci. Technol.* **2007**, *67*, 2528. (b) Ning, H.; Vaidya, U.; Janowski, G. M.; Husman, G. *Comp. Struct.* **2007**, *80*, 105.

(18) (a) Jen, A. K.-Y.; Lakshmikantham, M. V.; Albeck, M.; Cava, M. P.; Huang, W. S.; MacDiarmid, A. G. *J. Polym. Sci., Polym. Lett.* **1983**, 441–4. (b) Elsenbaumber, R. L.; Shacklette, L. W. *J. Polym. Sci., Polym. Phys.* **1982**, 1781–7. (c) Chance, R. R.; Shacklette, L. W.; Miller, G. G.; Ivory, D. M.; Sowa, J. M.; Elsenbaumer, R. L.; Baughman, R. H. *Chem. Commun.* **1980**, 348.

(19) Lee, H.-J.; Han, S.-W.; Kwon, Y.-D.; Tan, L.-S.; Baek, J.-B. *Carbon* **2008**, in press (DOI: 10.1016/j.carbon.2008.07027).

(20) http://www.iljinnanotech.co.kr.

(21) Frommer, J. E.; Chance, R. R. Electrically Conductive Polymers. In *Encyclopedia of Polymer Science & Engineering*, 2nd ed.; Mark, H. F., Bikales, N., Overberger, C. G., Menges, G., Kroschwitz, J. I., Eds.; Wiley: New York, 1986; Vol *5*, p 462.

(22) Sammaliorpi., M; Krasheninnikow., A.; Kuronen., A.; Nordlund., K.; Kaski., K. *Phys. Rev. B.* **2004**, *70*, 7.

(23) Baek, J.-B.; Tan, L.-S. *Polymer* **2003**, *44*, 4135.

(24) Allen, S. G.; Bevington, J. C. Poly(phenylene sulfide)s. In *Comprehensive Polymer Science*, 1st ed., Eastmond, G. C., Ledwith, A., Russo, S., Sigwalt, P., Eds.; Pergamon Press: New York, 1989; Vol 5, p 543.

(25) Fréchet, J. M. J. *Science* **1994**, *263*, 1710.

(26) Seo, K. H.; Park, L. S.; Baek, J.-B.; Brostow, W. *Polymer* **1993**, *34*, 2524.

(27) For recent reviews of hyperbranched polymers:(a) Gao, C.; Yan, D. *Prog. Polym. Sci.* **2004**, *29*, 183–275. (b) Jikei, M.; Kakimoto, M. *Prog. Polym. Sci.* **2001**, *26*, 1233. (c) Voit, B. *J. Polym. Sci. Part A: Polym. Chem.* **2000**, *36*, 2505. (d) Frey, H. *Angew. Chem., Int. Ed. Engl.* **1998**, 2193–2197. (e) Hult, A.; Johansson, M.; Malmström, E. *Adv. Polym. Sci.* **1999**, *143*, 1. (f) Hawker, C. J. *Adv. Polym. Sci.* **1999**, 113–160. (g) Kim, Y. H. *J. Polym. Sci. Part A: Polym. Chem.* **1998**, *36*, 1685. (h) Malmstrom, E.; Hult, A. *J.Macromol. Sci.-Rev. Macromol. Chem. Phys.* **1997**, *37*, 555. (i) Fréchet, J. M. J.; Hawker, C. J.; Gitsov, I.; Leon, J. W. *J. Macromol. Sci, Pure Appl. Chem.* **1996**, *A33*, 1399.

(28) Perloff, D. S. *Solid-State Electron.* **1977**, *20*, 681.

MA801259B